JOURNAL OF THE AMERICAN WATER RESOURCES ASSOCIATION

AMERICAN WATER RESOURCES ASSOCIATION

MAPPING RIVER BATHYMETRY WITH A SMALL FOOTPRINT GREEN LIDAR: APPLICATIONS AND CHALLENGES[1]

Paul J. Kinzel, Carl J. Legleiter, and Jonathan M. Nelson[2]

ABSTRACT: Airborne bathymetric Light Detection And Ranging (LiDAR) systems designed for coastal and marine surveys are increasingly sought after for high-resolution mapping of fluvial systems. To evaluate the potential utility of bathymetric LiDAR for applications of this kind, we compared detailed surveys collected using wading and sonar techniques with measurements from the United States Geological Survey's hybrid topographic/bathymetric Experimental Advanced Airborne Research LiDAR (EAARL). These comparisons, based upon data collected from the Trinity and Klamath Rivers, California, and the Colorado River, Colorado, demonstrated that environmental conditions and postprocessing algorithms can influence the accuracy and utility of these surveys and must be given consideration. These factors can lead to mapping errors that can have a direct bearing on derivative analyses such as hydraulic modeling and habitat assessment. We discuss the water and substrate characteristics of the sites, compare the conventional and remotely sensed river-bed topographies, and investigate the laser waveforms reflected from submerged targets to provide an evaluation as to the suitability and accuracy of the EAARL system and associated processing algorithms for riverine mapping applications.

(KEY TERMS: geographic information system; geomorphology; LiDAR; remote sensing; watershed management.)

Kinzel, Paul J., Carl J. Legleiter, and Jonathan M. Nelson, 2012. Mapping River Bathymetry with a Small Footprint Green LiDAR: Applications and Challenges. *Journal of the American Water Resources Association* (JAWRA) 1-22. DOI: 10.1111/jawr.12008

INTRODUCTION

The techniques used by fluvial scientists for collecting topographic and bathymetric measurements along river channels determine the scale over which physical processes and habitat conditions in these systems can be investigated. Cross-sectional surveys have been and continue to be an efficient technique for characterizing and monitoring stream reaches. However, the spacing of these cross-sections may not be adequate for representing critical details in the channel form that are important for understanding the steering of flow around bars or islands, exploring flood plain interactions, or defining mesoscale habitat. Significant progress has been made toward addressing these processes and conditions with increasing spatial detail. Therefore, it is becoming more common for fluvial scientists to collect spatially detailed datasets for mapping rivers and floodplains (Lane, 1994;

[1]Paper No. JAWRA-12-0109-P of the *Journal of the American Water Resources Association* (JAWRA). Received May 14, 2012; accepted September 20, 2012.

[2]Respectively, Hydrologist (Kinzel and Nelson), U.S. Geological Survey, Geomorphology and Sediment Transport Laboratory, 4620 Technology Drive, Suite 400, Golden, Colorado 80403; and Assistant Professor (Legleiter), Department of Geography, University of Wyoming, Laramie, Wyoming 82071 (E-Mail/Kinzel: pjkinzel@usgs.gov).

Brasington *et al.*, 2000; Hicks *et al.*, 2002; Tiffan *et al.*, 2002; Bowen *et al.*, 2002, 2003; Westaway, 2003; Lane, 2006; Hicks *et al.*, 2006; Lejot *et al.*, 2007; Legleiter and Kyriakidis, 2008; McKean *et al.*, 2008, 2009; Skinner, 2009, 2011).

The development of accurate, efficient, and cost-effective methods to collect continuous topography from a river bed to the drainage basin divide is a common goal shared among earth scientists. The technical, scientific, and engineering progress necessary for moving toward this goal continues to be stimulated from at least three principal drivers. First, much more detailed questions are being asked by river basin managers about the physical processes in rivers and streams and the relations of those processes to various critical issues, including flood inundation (Marks and Bates, 2000; Tayefi *et al.*, 2007), environmental flows for ecosystem support (Poff *et al.*, 1997; Richter *et al.*, 2006), and the evolution of channel form (Williams and Wolman, 1984; Collier *et al.*, 1996; Li and Millar, 2008). Consequently, there is a growing need to establish baseline conditions in river basins for the purpose of documenting future changes that may be brought about by either management decisions or as a result of natural disturbances. As an example, adaptive management (Holling, 1978; Walters, 1997) programs in river basins are undertaken with the goal of improving and/or protecting ecosystem condition. Management treatments to aid in species recovery in these basins may include such options as modifying the flow and/or sediment supplied to the river channel. Detecting the effects of these iterative restoration treatments through monitoring is an essential feedback mechanism in the adaptive management process.

Second, the need for detailed channel topography has been driven by the recent development of models, both physical and biological, which not only provide unprecedented predictive capabilities but also require detailed topographic input. For example, the assessment of local flood risk traditionally has been provided by one-dimensional models, which require only a few relatively widely spaced cross-sections. However, simulation of floodplain flows may be improved with two-dimensional models which require higher-resolution topography (Marks and Bates, 2000; Tayefi *et al.*, 2007). Similarly, biologists are increasingly moving away from habitat models based on reach-averaged quantities in favor of more complex models that require at least local depths and velocities (Waddle *et al.*, 2000; Tiffan *et al.*, 2002; Bowen *et al.*, 2003). Ecological simulations using individual-based models (Railsback *et al.*, 2003; Goodwin *et al.*, 2006) also require comprehensive characterization of the flow field.

Third, access to a particular area by surveyors may be complicated and impeded because of ownership or concern for the fragility of the riparian ecology. Detailed knowledge of denied access areas in fluvial environments also are of tactical and strategic importance to the armed forces for shallow water operations.

Over the past 15 years, considerable research attention has been focused on the use of remote sensing for collecting bathymetry in rivers and streams (Marcus and Fonstad, 2010). These techniques include extending the use of photogrammetry to water bodies by correcting for refractive effects (Westaway *et al.*, 2003). Passive optical approaches, which derive a relationship between the amount of reflected sunlight from the river bottom and the overlying water depth, were used in empirical (Winterbottom and Gilvear, 1997; Carbonneau *et al.*, 2006; Lejot *et al.*, 2007) and more physics-based models (Legleiter *et al.*, 2004, 2009). Optical approaches, however, are constrained by the visibility of the river bottom in the imagery, and relating image-derived quantities to flow depths typically requires site-specific field calibration. Additionally, if an automated georeferencing process cannot be used, a ground control network may be required to orient the imagery (Lejot *et al.*, 2007), and installing a dense network for this purpose may not be practical for synoptic mapping projects that extend over many kilometers. The reflectance from a river also depends on sun angle, atmospheric characteristics, surface waves, turbidity, and heterogeneous bottom reflectivity, and spatial and temporal variations in these quantities must be taken into account as well (Legleiter *et al.*, 2009).

Alternatively, active remote-sensing techniques such as Light Detection And Ranging (LiDAR or lidar, also known as airborne laser swath mapping) have been applied along rivers (Marks and Bates, 2000; Hicks *et al.*, 2002; Bowen and Waltermire, 2002; Tiffan *et al.*, 2002; Hicks *et al.*, 2006; Tayefi *et al.*, 2007; Höfle *et al.*, 2009). Airborne LiDAR systems precisely determine the round-trip time for a laser pulse emitted from a sensor on an aircraft to reach a reflective surface, such as vegetation or the ground, and return back to the aircraft. The laser range is computed by halving the product of the round-trip travel time and the speed of light through the transmission media. The airborne sensor's position and orientation at the time of each laser pulse are determined from postprocessed data from an integrated global-positioning system (GPS) and an inertial measurement unit (IMU) system; these data are combined with laser range and scan angle data to calculate the 3D spatial coordinates of the laser reflections from the earth's surface. An increase in the number of commercially available topographic LiDAR sensors over the last decade has made this technology cost-efficient for mapping large areas. To

date in fluvial settings, LiDAR sensors have most often been utilized to obtain subaerial or exposed topography using data collected with discrete return topographic LiDAR systems that operate at a wavelength of 1,064 nm. This near-infrared radiation is strongly absorbed by the water column, preventing a usable signal return, which effectively precludes these systems from making bathymetric measurements. Depending on the particular system and water conditions, infrared LiDAR reflections near the water surface can occur from waves or turbidity (Huising and Gomes Pereira, 1998) or the laser energy transmitted to wetted areas is completely absorbed and does not return to the aircraft resulting in laser shot dropouts (Höfle *et al.*, 2009).

For the purposes of this study, we consider bathymetric LiDARs as those that have water-penetrating capabilities. Bathymetric LiDARs have lasers that operate in the green region of the electromagnetic spectrum, typically 532 nm using a frequency-doubled Nd:YAG laser. Because the laser power from this wavelength is less attenuated than near-infrared lasers, green LiDARs are capable of greater penetration of the water column and recovery of reflections from the channel bed. However, the transmission of the laser pulse through water depends on various environmental conditions that can influence the strength and shape of the laser pulse that is returned to the aircraft. The most significant parameter-limiting depth penetration for these systems is water clarity, which causes absorption (energy reduction) and scattering (energy redistribution) of the pulse (Guenther, 2007). Suspended sediments, organic particulates, and dissolved organic and inorganic material can all affect the optical properties of the water column. Other environmental factors that affect the laser pulse include the water surface (waves), aeration in the water column that also can cause absorption and scatter, and vegetation. The composition and roughness of the channel bottom, with regard to substrate size, may also have a role on the reflectivity. Shallow depths also present a challenge because of the difficulty in separating water surface, water column, and bottom reflections all closely spaced in time (Kinzel *et al.*, 2007). Because of these complexities, the entire time history of the laser pulse or waveform is digitized by the bathymetric system to aid in postprocessing. This is less commonly done in topographic mapping LiDARs, which typically record only a few discrete returns of the reflected waveform.

Currently, bathymetric LiDAR systems remain highly specialized pieces of instrumentation. Some examples and commercial manufacturers of these systems include the Hawk Eye II (Airborne Hydrography, Sweden), the Laser Airborne Depth Sounder (Tenix LADS Corporation, Australia), and the Scanning Hydrographic Operational Airborne LiDAR System (SHOALS) (Optech, Canada). The Hawkeye II system has been recently used in the Gardon River in France (Bailly *et al.*, 2010). One of the first bathymetric LiDAR surveys in a river was conducted in 1998 using the SHOALS instrument in the Hanford reach of the Columbia River (Tiffan *et al.*, 2002). Recently, a newer version of the SHOALS instrument, the 1000T was used to survey the Yakima River in Washington and the Trinity River in California (Hilldale and Raff, 2008) and the Colorado River below Glen Canyon Dam in Arizona (Millar, 2008). Hilldale and Raff (2008) concluded, for the two rivers they examined, that the SHOALS 1000T performed within expected levels of precision but had a systematic bias to measure river-bed elevations above ground-truth elevations.

The bathymetric LiDARs in the above examples were designed to optimize depth penetration, using high power to overcome the problems associated with recovering the laser pulse in deep, possibly highly attenuating water. However, the high power ($\sim$5,000 μJ per pulse) of these bathymetric LiDARs imposes a fundamental design constraint on the footprint of the laser spot to ensure eye-safe operation for individuals on the ground. Consequently, a spot size of a few meters in these systems is necessary to reduce the energy to the level at which eye safety is achieved. Although this design is satisfactory for marine surveys, typically conducted in depths on the order of tens of meters, shallow water (<10 m) performance is sacrificed with regard to spatial density and resolution (Wright and Brock, 2002; Hildale and Raff, 2008; Allouis *et al.*, 2010). Therefore, these bathymetric LiDAR designs are not optimized for providing the spatial resolution necessary for mapping small to medium-sized rivers. Aside from the design constraints, other factors have hampered operational demand and associated technological development of these systems for fluvial environments. These factors include the relative scarcity of bathymetric LiDAR systems, as compared with topographic systems, LiDAR mobilization cost, and expenses related to the acquisition and processing of the data.

However, the interest in mapping fluvial environments with bathymetric LiDAR has accelerated in recent years and a number of next-generation systems are currently being developed and field tested. Thus, the intent of this article is to (1) briefly describe a single-frequency bathymetric Experimental Advanced Airborne Research LiDAR (EAARL) that uses a smaller laser footprint and narrower pulse width than past bathymetric LiDAR designs, (2) describe the algorithms that have been and are currently used to process EAARL waveforms collected in

shallow fluvial environments, and (3) evaluate the performance of these algorithms by assessing bathymetric mapping accuracy along three riverine study sites of varying water clarity, bed configuration, and bottom type.

METHODS

EAARL Hardware

The hardware that currently makes up the EAARL system has been described previously (Wright and Brock, 2002; Nayegandhi *et al.*, 2006; Kinzel *et al.*, 2007; McKean *et al.*, 2009; Nayegandhi *et al.*, 2009), and only an abbreviated description is included herein. The EAARL laser transmitter is a Continuum EPO-5000 doubled YAG laser (Continuum, Santa Clara, CA) that has been flown on a Cessna 310 aircraft and most recently deployed on a Pilatus PC-6 at a nominal altitude of 300 m. At this altitude, a scanning mirror directs a laser swath that measures approximately 240 m across with a laser sample every $2\text{ m} \times 2\text{ m}$ along the center and $2\text{ m} \times 4\text{ m}$ along the edge of the swath. The area illuminated by each laser sample on the ground is approximately 0.2 m in diameter. The position of the EAARL laser samples are determined using two high-precision, dual-frequency kinematic carrier phase GPS receivers and an integrated miniature IMU. These instruments provide submeter horizontal geolocation for each EAARL laser sample (Wright and Brock, 2002; Nayegandhi *et al.*, 2006; Nayegandhi *et al.*, 2009). The EAARL pulse energy is only 70 μJ per pulse, about 1/70th the power of other bathymetric LiDARs allowing eye safe operation at a much narrower field of view (Feygels *et al.*, 2003). The EAARL also operates at a pulse repetition frequency between 3,000 and a maximum of 5,000 Hz. Each transmitted green (532 nm) laser pulse is 1.2 ns in duration, narrower than most bathymetric LiDARs, corresponding to a travel distance of approximately 0.15 m in air and 0.11 m in water. The short pulse of the EAARL system is thought to improve shallow depth determination (Nayegandhi *et al.*, 2009; Allouis *et al.*, 2010). The system is capable of storing the entire time series of backscattered laser energy reflected from targets using an array of four high-speed waveform digitizers connected to four subnanosecond photodetectors. The photodetectors vary in sensitivity, with the most sensitive channel receiving 90% of the reflected photons, the middle channel receiving 9%, and the least sensitive 0.9%. A fourth channel is also available for Raman or infrared backscatter. This range in detector sensitivities is important since targets along a flight path can vary in physical and optical characteristics, influencing the intensity and structure of the reflected laser waveform.

EAARL Postprocessing Software

In addition to the hardware design, another significant departure of the EAARL from other bathymetric systems is the creation of a freely available software product for LiDAR processing. The Airborne Lidar Processing System (ALPS) (U.S. Geological Survey, St. Petersburg, FL) is the result of collaboration between the National Aeronautics and Space Administration and U.S. Geological Survey (USGS). The software allows scientists to interact with data from EAARL missions to obtain topographic and bathymetric information using a suite of waveform-processing algorithms (Nayegandhi *et al.*, 2006; Bonisteel *et al.*, 2009; Nayegandhi *et al.*, 2009). Using this type of open-source software has a number of advantages. The ALPS-processing software can be easily distributed, updated easily with each new version, and even modified by the user community. LiDAR data are almost exclusively processed by the vendor and the deliverables may include points, surfaces, or breaklines. Technical details of the LiDAR-processing routines from commercial vendors are typically proprietary and consequently not shared with the customer. The ALPS interface provides a tool for scientists to interact with data collected during an EAARL survey. Users can view the natural color and color infrared imagery collected during the flight, select flight lines, view the laser swaths along a flight line, interrogate and plot individual laser waveforms in each flight line, apply processing algorithms to the waveforms to construct surfaces, and apply filters to remove false bottom returns and outliers from the dataset (Bonisteel *et al.*, 2009). Processing algorithms in ALPS currently provide for the computation of a first-return surface, a last-return surface (bare earth), and submerged surfaces.

The EAARL data collected from our study reaches were processed using the ALPS software package, and maps of river channel topography were created with the ALPS waveform-processing algorithms. One of these algorithms, the first-surface algorithm, computes the range using the zero-point crossing of second derivative of the waveform (Bonisteel *et al.*, 2009). The first-surface algorithm can be used to detect the location of a surface reflection in waveforms returned from subaerial targets along riverine and coastal areas. The first-surface algorithm is also presently used to ascertain the first reflection in an EAARL bathymetric waveform. This point could

mark the transition from the laser travel from air to water, in the case of a true specular reflection, or depending on the incident angle might correspond to a reflection further into the water column. The elevation of the bottom in an EAARL bathymetric waveform is found by correcting for the angle of refraction of the incident laser pulse at the air-water interface, accounting for the change in the speed of light as it enters the water column, the attenuation of the laser signal in water, and the effect of water-column turbidity on the laser backscatter (Nayegandhi *et al.*, 2009). In coastal open-water applications, the air-water interface is found in ALPS by identifying strong Fresnel reflections that occur near nadir in the most sensitive waveforms channel. This technique is not typically employed for rivers because of the relative paucity of Fresnel reflections over the much narrower wetted portion of the surveyed swath.

The bathymetry algorithm used in ALPS versions prior to June 2011 was designed to detect the location of a bottom return in waveforms returned from shallow depths, typically <1 m, as well as strong bottom returns from deeper depths. This algorithm is referred to by the authors as the maximum peak (MP) because, after the waveform is corrected for laser and water column decay effects, the algorithm selects the most significant, highest intensity peak after the initial reflection. Figures 1A to 1C show the reflected waveform (thick black line) displayed in ALPS from various targets. The colored lines indicated the effect of the variables used in the bathymetry algorithm when they are applied to the backscattered waveform. Figure 1A shows a reflection from an emergent target. As compared with the single peak in the emergent target, waveforms from submerged water targets (Figure 1B) can exhibit multiple peaks that display a separation between the initial reflection and a subsequent peak(s), which may have contribution from the bottom. The shape of a more complex shallow-water waveform (Figure 1C) results from the interaction of multiple returns that may include the water surface, water column reflectors that may be due to turbidity, and reflections from the river bed all closely spaced in time. Once corrected for laser column and water decay effects, the MP algorithm searches for the most significant peak along the trailing edge of the waveform. This location is shown with an inverted blue triangle in Figures 1B and 1C.

The second bathymetry algorithm and the technique implemented in the version of ALPS released after June 2011 implements a different approach for selecting the bottom. This technique is referred to by the authors as the last peak (LP) bathymetric algorithm. The LP algorithm like the MP algorithm first corrects the waveform for laser and water column

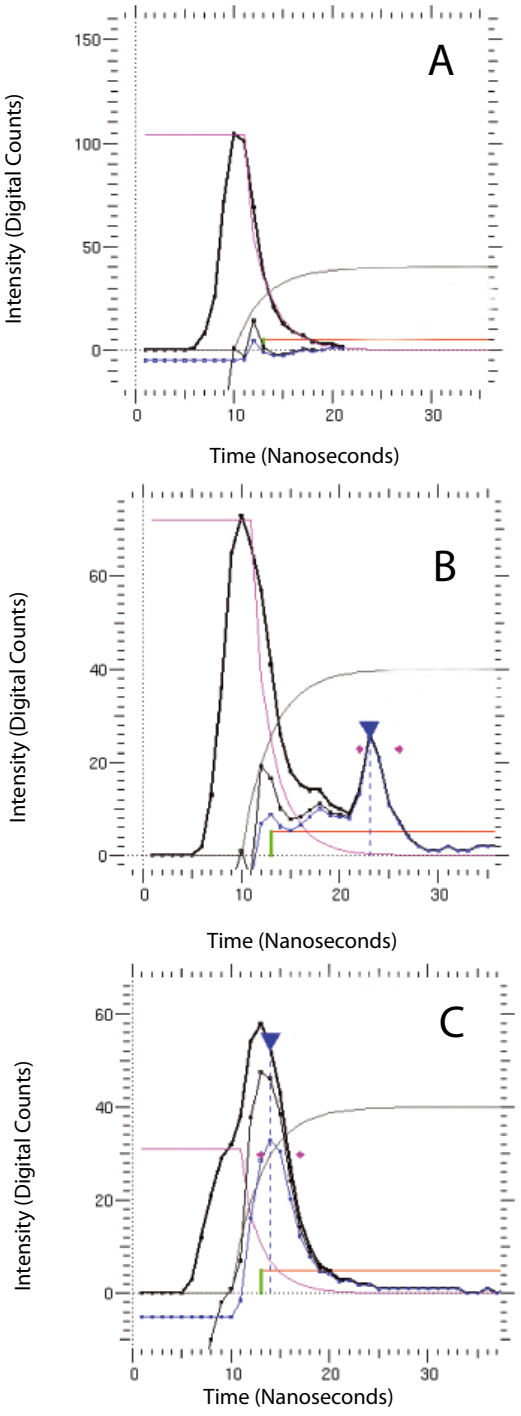

FIGURE 1. Example Waveforms (thick black lines in each panel) from an Emergent Target (A), a Submerged Target (B), and a Shallow Submerged Target (C). Lines illustrating the parameters used by the Airborne Lidar Processing System (ALPS) bathymetry algorithm are also shown in each panel. The green and red lines mark the interval over which a bottom reflection is expected. The magenta line is the exponential decay. The thin black line is the exponential equalizer function. The blue line is the result of subtraction of the exponential decay from the original waveform and multiplication of the exponential equalizer. Blue inverted triangles, if present, mark the location of the last return, the peak of the blue trace. Note: Different scales are used to enhance resolution.

decay but instead of selecting the highest peak value after the initial peak, this algorithm finds all inflection points in the waveforms using the first derivative and selects the last peak above a threshold value. This change was made to reduce the likelihood of selecting a stronger peak from the turbidity reflection over a much weaker bottom reflection. The result of using these two algorithms on sample waveforms are shown and discussed later in the results section of the article.

ALPS allows the user to interactively adjust the parameters of the bathymetric algorithm while processing the LiDAR waveforms (Bonisteel *et al.*, 2009). The application of the bathymetric algorithms to the example waveforms are also shown in Figures 1A to C. The shape of an exponential decay function (magenta line) is adjusted to follow the trailing edge of the waveform (thick black line). The exponential decay function is a combination of the attenuation of the laser pulse and the pulse stretching caused by slower travel through the water column. The laser and water exponential constants and other processing parameters are set by the ALPS user (Table 1). The combined decay function is subtracted from the waveform and the result multiplied by an exponential equalizer function (thin black line) also referred to as the automatic gain control (AGC). The purpose of the exponential equalizer is to equalize the bottom signal strength and reduce the likelihood that noise in the water column is detected over a weaker bottom signal. The blue trace is the final result after the exponential equalizer has been applied. The peak of the blue trace is an estimate of the location of the bottom, which is also shown on the original signal with a blue triangle. The user can also set the locations in the waveform where the algorithm will begin to search for a last reflection (first) and stop searching (last), similar to a range gate. Other parameters include a threshold value (Thresh) that is used to set the number of digital counts below which the algorithm considers noise and Max Sat that refers to the maximum number of points that can be saturated in a return channel before the next sensitive channel is selected. Note that the algorithm does not detect a bottom reflection in Figure 1A in the single peak from the emergent target but finds the location of a bottom reflection in Figures 1B and 1C. The location of the peak of the initial reflection is determined from the zero-point crossing of second derivative of the waveform similar to the first-surface approach. The bathymetry algorithm determines the total range to the river bottom by first computing the range vector from the sensor to the first surface using the two-way speed of light in air (15 cm/ns) and then calculates the portion of the range vector through the water using the two-way speed of light through water (11 cm/ns) and correcting for refraction.

TABLE 1. Settings Used for the ALPS Bathymetry Algorithm, see Bonisteel et al. (2009).

Feature	Setting
Laser	−3.8
Water	−4
AGC	−3
Thresh	3
First	13
Last	60
Max Sat	2

Notes: Laser, the exponential decay due to the laser attenuation in water; Water, the exponential decay over the water column; AGC, automatic gain control, an exponential equalizer; Thresh, threshold above which the digital counts in the return are considered valid; First, the point in the return waveform where the algorithm searches for a first surface return; Last, the point in the return waveform where the algorithm stops looking for a bottom return; Max Sat, the maximum saturation of a return that is acceptable.

As the algorithms used to process a LiDAR survey can have a significant influence on the accuracy of the data produced, we sought to examine the performance of the EAARL sensor and the ALPS algorithms in three fluvial study areas with various water column characteristics and substrate types. Although the EAARL data collected for this study predated the ALPS version released in April of 2010, significant changes were made to the bathymetric algorithm in June 2011. These changes were distributed in the second ALPS version, released in November of 2011. Both versions of ALPS (April, 2010 and November, 2011) were used in the processing of data from our study sites and the bathymetric settings used for both versions are shown in Table 1. Of particular interest is the threshold value which when adjusted in the latter release has a stronger influence on determining the location of the last return in a bathymetric waveform. The bathymetric settings in Table 1 were determined by comparing samples of ground-truth data on the Trinity River to nearby waveforms that were digitized by the EAARL. These settings were then used by the developers of ALPS to process waveforms from the Trinity and the Klamath Rivers and in the construction of the final deliverable products. These settings are also similar to the shallow riverine preset settings that would be available for use in ALPS and therefore might serve as an initial starting point for processing of river bathymetry. Instrument roll bias was determined and corrected for the Trinity and Klamath Rivers and these values were used in our subsequent ALPS processing. For the Colorado River survey, roll bias for the instrument was computed using opposite flightlines that overlapped a bridge.

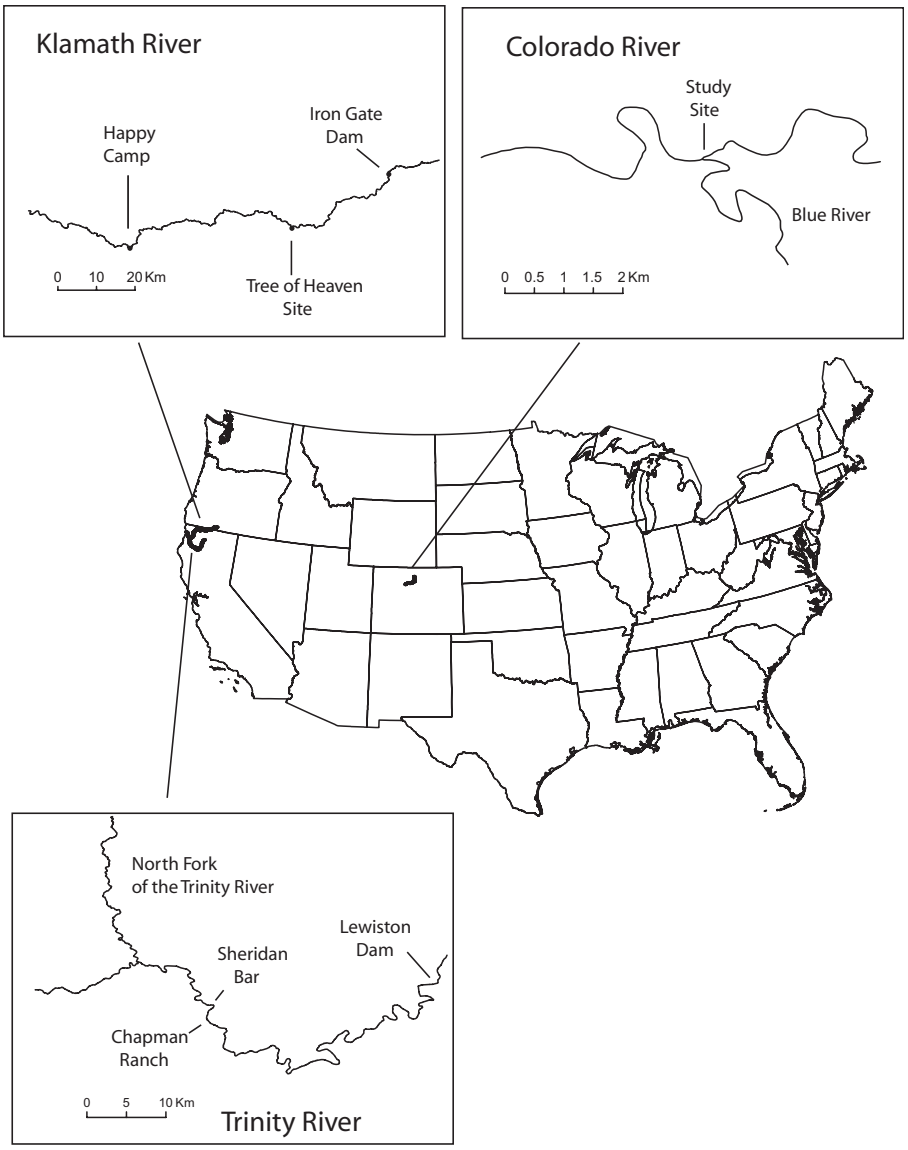

FIGURE 2. Map Showing the Rivers and Location of Study Sites Surveyed with the EAARL System.

STUDY AREAS

Trinity River, California

The Trinity River is a gravel-bedded river located in northern California (Figure 2, Table 2). A major tributary to the Klamath River that in turn drains to the Pacific Ocean, the Trinity River, is thought to have historically supported large populations of salmon and steelhead. Since 1963, the Trinity River Diversion, completed as part of California's Central Valley Project, has withdrawn up to 90% of the average annual yield of the Trinity River. The Trinity River Flow Evaluation Study, completed in 1999, determined that reductions in river flows from the Trinity River Diversion were responsible for subsequent declines in salmon and steelhead (U.S. Fish and Wildlife Service and Hoopa Valley Tribe, 1999). This study also provided the impetus for the Trinity River Restoration Program (TRRP), which seeks to restore salmon and steelhead populations in the river.

The channel and floodplains of the Trinity River have also been altered by gold and gravel mining operations (Krause *et al.*, 2010). In addition to flow and sediment management activities, TRRP intends to construct 47 channel rehabilitation sites in the floodplain of the Trinity River. Rehabilitation will involve the removal of fossilized riparian berms along

TABLE 2. Characteristics of the Study Reaches.

Study Reach, River	Length (km)	Mean Depth (m)	Mean Width (m)	Bed Material	Turbidity* (NTU)	SSC† (mg/l)
Sheridan Bar, Trinity	1.1	0.95	36	Gravel	<2	NA
Chapman Ranch, Trinity	0.8	1.09	29	Gravel	<2	NA
Tree of Heaven, Klamath	0.4	1.84	39	Bedrock/gravel/sand	3	<3
Confluence, Blue/Colorado	1.4	0.91	57	Sand	~6	3-10

Note: NTU, Nephelometric Turbidity Unit.

*Turbidity values for the Trinity River were obtained from the California Department of Water Resources web site; turbidity on the Klamath was measured with a HF Scientific DRT-15CE Turbidimeter (HF Scientific, Fort Myers, FL); turbidity on the Colorado was measured with a Eureka Environmental Manta 2 (Eureka Environmental, Austin, TX).

†Suspended sediment concentrations on the Klamath River were determined by the Redwood National Park Laboratory, Orick, California; suspended sediment concentrations on the Blue/Colorado were determined by the U.S. Geological Survey Iowa Sediment Laboratory, Iowa City, Iowa.

the banks of the river to increase floodplain connectivity and enhance aquatic and riparian habitat. In April of 2009, USGS in cooperation with TRRP surveyed 68 km of the Trinity River between Lewiston Dam and the North Fork of the Trinity River with the EAARL instrument (Figure 2). The EAARL survey was acquired to augment a synchronized terrestrial LiDAR data collection providing seamless digital elevation data of the river and floodplains that could aid in the design and construction of channel rehabilitation sites.

Two study sites were selected along the Trinity River and surveyed to evaluate the mapping accuracy of the EAARL. The Sheridan Bar site (Figure 2), a rehabilitation site, was selected due to the bar-pool morphology and because it had been examined previously in a study of the effects of bed mobility on salmon-spawning suitability (May *et al.*, 2009). The Chapman Ranch site, Figure 2, approximately 1.3 km upstream of Sheridan Bar, was also selected for evaluation. A combination of wading with real-time-kinematic (RTK) GPS or a robotic total station (TS), and RTK GPS-enabled single-beam sonar for deeper areas were used to map the sites. The manufacturer-reported precisions of RTK measurements are approximately ±2 cm in the vertical and ±1 cm in the horizontal (Trimble Navigation Limited, 1998). Sonar measurements were made using an Innerspace Model 448 echosounder (Innerspace Technology, Inc., Carlstadt, NJ) that can resolve depths to a precision of approximately 3 cm. Ground-based measurements were spatially referenced using benchmarks with coordinates determined by TRRP in the NAD83 horizontal datum and GRS80 ellipsoid. The ground-truth bathymetry measurements were collected in a somewhat random manner, we did not adhere to any formal protocol regarding the point density sampled or spacing of cross-sections. Overall, the goal of the ground-truth surveys was to collect to the extent possible a spatial distribution of bathymetric measurements that could be used to characterize the morphology of the river reaches, specifically in the areas of deep pools. The EAARL data were first processed by USGS personnel in St. Petersburg, Florida, using the ALPS software. The EAARL survey along the Sheridan Bar and Chapman Ranch reaches that was delivered to TRRP and used in our statistical analysis, and described in the results section, included only points collected in the wetted channel on the multiple days when flight lines overlapped this area (Table 3). Although LiDAR points outside the channel were collected with the EAARL system, they were not used in our statistical comparisons. We also used the ALPS software to process the flightlines over the Sheridan Bar collected during a single day of the EAARL survey (April 17, 2009). This was done to retrieve not only the last-return elevations, but also the first-return elevations and the structure of the return waveforms that were collected near a transect. This approach allowed us to directly compare all of the EAARL measurements made on that day with the ground-based measurements made along a transect.

The turbidity of the Trinity River was <2 Nephelometric Turbidity Units (NTUs) at the Limekiln Gulch streamflow-gaging station, which is located approxi-

TABLE 3. EAARL Data Collection Parameters.

Study Reach	Date(s)	Flightlines	Point Density (no. pts/m^2)
Sheridan Bar, Trinity	April 16-20, 2009	17	0.45
Chapman Ranch, Trinity	April 16-20, 2009	14	0.67
Tree of Heaven, Klamath	April 21, 2009	6	0.03
Confluence, Blue/Colorado	October 3, 2009	19	0.34

mately 20 km upstream of the study reaches (Table 2) (California Department of Water Resources, California Data Exchange Center, http://cdec.water.ca.gov/, *accessed* August 16, 2012). The discharge varied from 15 to 17 m^3/s at the Trinity River at Junction City streamflow-gaging station located 3 km downstream of the Sheridan Bar reach (USGS, National Water Information System, http://waterdata.usgs.gov/nwis, *accessed* August 16, 2012; unless otherwise noted all streamflow data in this article are accessed from this source). The water was clear and surveyors collecting wading measurements had no difficulty in resolving the river bottom. Secchi disks lowered in pool locations throughout the EAARL surveyed reach and coincident in time with the EAARL survey were visible at depths up to about 3 m.

Klamath River, California

After the Trinity River survey, the EAARL was deployed to the Klamath River for a single day of surveying on April 21, 2009. The EAARL survey was in support of a USGS multidisciplinary project with flight lines extending downstream from Iron Gate Dam to the town of Happy Camp, California (Figure 2). Concurrently, a ground survey using RTK GPS, sonar, and a TS was collected in the town of Happy Camp at the confluence of the Klamath River and Indian Creek. The portion of the EAARL survey overlapping this ground-truth location was later determined to be unusable because of a malfunction in the EAARL IMU. Consequently, a replacement ground survey was collected at the Tree of Heaven study site on August 26-27, 2010, which overlapped a region of the EAARL data collection where the IMU functioned properly (Figure 2). In this reach, the river bed is composed of bedrock in the thalweg with gravel and cobbles and sand along the right bank. An acoustic Doppler current profiler (Mueller and Wagner, 2008) coupled with an RTK GPS was used to map the river bottom. The datum used for this survey was relative to the ITRF00/WGS84 ellipsoid. As with the Trinity River surveys, we collected data in a somewhat random fashion with a similar goal of achieving a spatial coverage that represented the morphology of the reach.

Like the Trinity River, the Klamath River had relatively low turbidity ~3 NTU, and the suspended sediment concentration was <3 mg/l during the EAARL flight (Table 2). The mean daily discharge on the day the EAARL was flown was 45 m^3/s at the Klamath River below Iron Gate Dam, located 26 km upstream of the Tree of Heaven study site (Figure 2). At the time of the subsequent ground survey, the discharge was approximately 40 m^3/s. The difference in stage at these two discharges at the Iron Gate Dam streamflow-gaging station is <0.1 m. Water clarity observations were not available at the time of the EAARL survey at the Tree of Heaven site. However, simple visual observations made at the time of the subsequent ground survey were unable to resolve the river bottom in all but the shallowest (<0.5 m) areas along the channel margin.

Confluence of the Blue and Colorado Rivers, Colorado

The Colorado River near Kremmling is a popular location for fishing and rafting in Colorado's high country. The Blue River enters the Colorado from the south (Figure 2) and is regulated by Green Mountain Reservoir approximately 20 km upstream of the confluence. Portions of the Colorado and Blue Rivers in this area have been deemed eligible for wild and scenic designation due to outstanding recreation, wildlife, and biodiversity values (U.S. Department of the Interior Bureau of Land Management, 2007). This reach was selected for evaluation because of the unique river confluence morphology. The bed material of both rivers is predominantly sand, and aquatic vegetation was present in shallow areas along the channel margins. Suspended sediment samples were collected on the day of the EAARL survey using a hand-held DH-48 sampler. The sampler was designed by the Federal Interagency Sedimentation Project (FISP) http://water.usgs.gov/fisp/products/4101002.html. The average suspended sediment concentration for the Colorado River was 4 mg/l, standard deviation (SD) = 3 mg/l (n = 3), and for the Blue River 10 mg/l, SD = 7 mg/l (n = 3) (Table 2). The water was thus relatively clear and the river bed was visible through depths up to approximately a meter in both rivers. Turbidity data collected was not collected during the EAARL flight. However, subsequent measurements made in October of 2011 on the Blue River and at a suspended sediment concentration of 8 mg/l had a mean value of 6.1 NTU and SD of 1.6 NTU.

Topographic and bathymetric surveys were collected using similar methods and mapping objectives as those used on the Trinity River and were conducted on September 18-20, 2009. The mean daily streamflow at the Kremmling streamflow-gaging station, located on the Colorado River approximately 5 km downstream from our study reach, was 29 m^3/s. The datum used for this survey was relative to the ITRF00/WGS84 ellipsoid. The EAARL survey was collected on October 3, 2009, over a period of about 1.5 h when the discharge was approximately 30 m^3/s. LiDAR data were collected along 19 flightlines over the Colorado and Blue Rivers (Table 3).

TABLE 4. Statistical Comparison of Points <0.5 m Apart.

Study Reach, River	Survey Method	*n*	ME	RMSE	SD
Sheridan Bar, Trinity*	Sonar	2,890	0.38	0.52	0.36
	Wading	610	0.27	0.34	0.21
Chapman Ranch, Trinity*	Sonar	5,296	0.32	0.38	0.21
	Wading	632	0.17	0.25	0.19
Tree of Heaven, Klamath†	Sonar	385	0.32	0.76	0.68
Confluence, Blue/Colorado	Sonar	5,988	0.08	0.15	0.13
	Wading	271	0.07	0.14	0.12

Notes: Colorado River comparisons used the EAARL data processed by the authors using the last peak bathymetry algorithm and a threshold value of 5.

*Trinity River comparisons used the EAARL data delivered to TRRP that was processed with the maximum peak bathymetry algorithm.

†Klamath River comparisons used the EAARL data delivered to USGS using the last peak bathymetry algorithm and a threshold value of 3.

RESULTS

Trinity River – Sheridan Bar and Chapman Ranch Sites

The elevations of the EAARL data processed by the USGS in St. Petersburg tended to lay above the elevations of ground survey data at the Sheridan Bar and Chapman Ranch sites. Comparison of 610 wading measurements surveyed with RTK GPS in the Sheridan Bar reach and EAARL survey heights located within 0.5 m of the field data showed the mean error (ME), defined as EAARL-ground) was 0.27 m, the root mean square error (RMSE) was 0.34 m, and the standard deviation (SD) was 0.21 m (Table 4). The paired sonar measurements also showed a positive ME at the Sheridan Bar site, 0.38 m, RMSE of 0.52 m, and an SD of 0.36 m. Results from the wading measurement comparison at the Chapman Ranch site indicated a somewhat lower ME of 0.17 m and RMSE of 0.25 m as compared with the Sheridan Bar site. Sonar comparisons from this site were also somewhat lower than for the Sheridan Bar site, ME of 0.32 m and RMSE of 0.38 m.

Although these reach aggregated values provide some insight into the accuracy and precision of the dataset delivered to TRRP, we sought to explore in more detail the performance of the system in an area that was not well resolved in the deliverable EAARL survey. This area was a deep (>4-m) pool in the Sheridan Bar reach. Figure 3A, created from data collected on April 17, 2009, and processed using the MP bathymetric algorithm, illustrates how the elevation contrast between the deeper portions of the pool shown in the ground sonar-based survey (Figure 3B) was not captured in the EAARL survey processed with this algorithm. Examination of EAARL waveforms returned from this pool on April 17, 2009, indicated that the maximum separation between the first-surface and bottom-surface elevations was only 2.3 m. It should be noted here that these EAARL waveforms were processed and are presented without automatic or manual filtering. This was done because we found the filtering techniques tended to smooth what was a relatively sparse dataset collected on a single day. For comparison, we reprocessed the EAARL data from the same day using the LP bathymetric algorithm, the current technique to identify bottom returns in the ALPS software (Figure 3B). A threshold value of 3 was used in the processing to be consistent with ALPS-processing settings that were subsequently used with the LP algorithm applied to the Klamath River dataset and settings that were used in the deliverable dataset to the TRRP and processed using the MP algorithm (Table 1). We then compared the surveys along a transect, line T to T′, immediately downstream of the pool by selecting and plotting the EAARL and ground-surveyed sonar points within 0.5 m of the transect line (Figure 4). To reduce any vertical bias between the surveys, we used the elevations collected by the EAARL on an emergent gravel bar and compared them with adjacent ground-surveyed points to block correct the first- and last-return elevations computed by the ALPS software. The effects of the two bathymetric processing algorithms on the shape of a river cross-section defined from the EAARL survey are shown in Figure 4A. In the case of the MP algorithm, the elevation of the cross-sectional profile derived from the EAARL data was higher than that measured by the ground survey. To illustrate the reason for this difference in a simple manner and to visualize the time history of laser intensity on a pulse, we examined a raster plot that crossed the pool (Figure 4B). The vertical axis in the raster plot represents the intensity returned to the detector every nanosecond in the pulse. The pulses along the scan line or raster are then stacked side by side along the horizontal axis of the plot. The warmer colors represent a higher magnitude intensity than the cooler colors. It is important to note that the raster selected, 119459, is a single scan line and the points on Figure 4A also include pulses from other rasters that fell within the 0.5-m search radius. Raster 119459 has high-intensity reflections in pulses 75 to 78 that occur between 10 and 15 ns. Closer inspection of these pulses indicates weaker reflections occurring between 35 and 40 ns. We then examined a single pulse or waveform marked with "T1" in Figures 4A and 4B. This waveform shown in Figure 4C has a strong initial reflection at 98 digital counts and subsequent inflections at

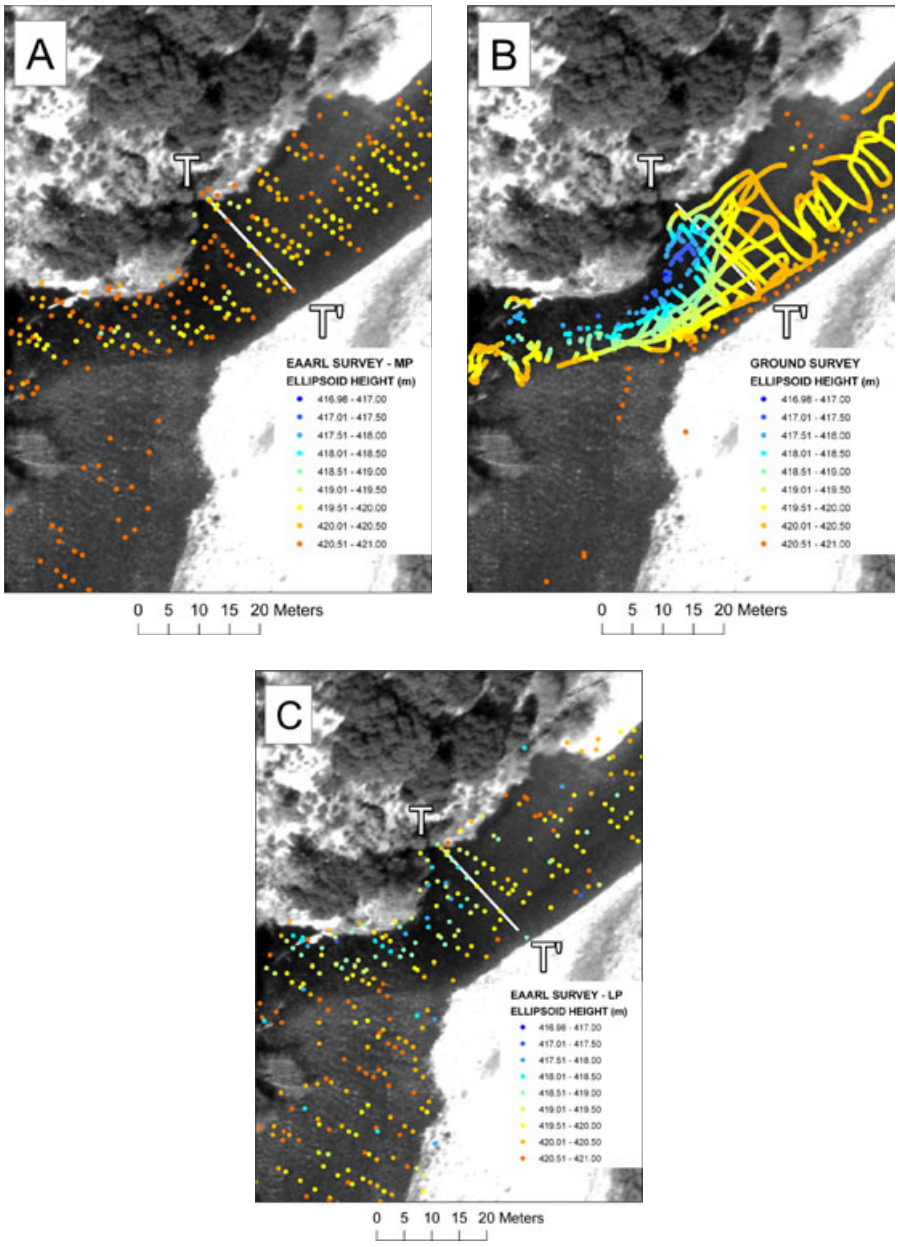

FIGURE 3. Bathymetric Surveys of the Trinity River: (A) Bathymetric Points Collected with the EAARL and Processed with the ALPS Maximum Peak (MP) Bathymetry Algorithm; (B) Bathymetric Points Collected with Ground-Truth Surveys; (C) Bathymetric Points Collected with the EAARL and Processed with the ALPS Last Peak (LP) Bathymetry Algorithm. Sheridan Bar study site, Trinity River, California. Flow is from lower left to upper right.

22, 10, and 14 digital counts. When processed with the MP bathymetric algorithm, the inflection in the waveform with a magnitude of 22 digital counts at 17 ns was identified as the bottom because it exceeded the magnitude of all subsequent inflections. However, when the LP algorithm was used, the reflection with a magnitude of 14 digital counts at 36 ns was selected because it was the last inflection that exceeded 3 digital counts. Apart from the vertical differences, the comparison between EAARL and ground elevations at this transect also suggests an imprecision in the horizontal positioning between these surveys. This may have been because the plane was banking in the area of the Sheridan Bar pool, and although a roll bias value was used to correct the entire survey, it may have not been suitable for this time and location. It is also interesting to note that shallower points identified by the MP algorithm along river right (as viewed looking downstream) were not identified by the LP algorithm. In addition to these omissions, other points identified by the LP algorithm resulted in an overprediction of depth especially

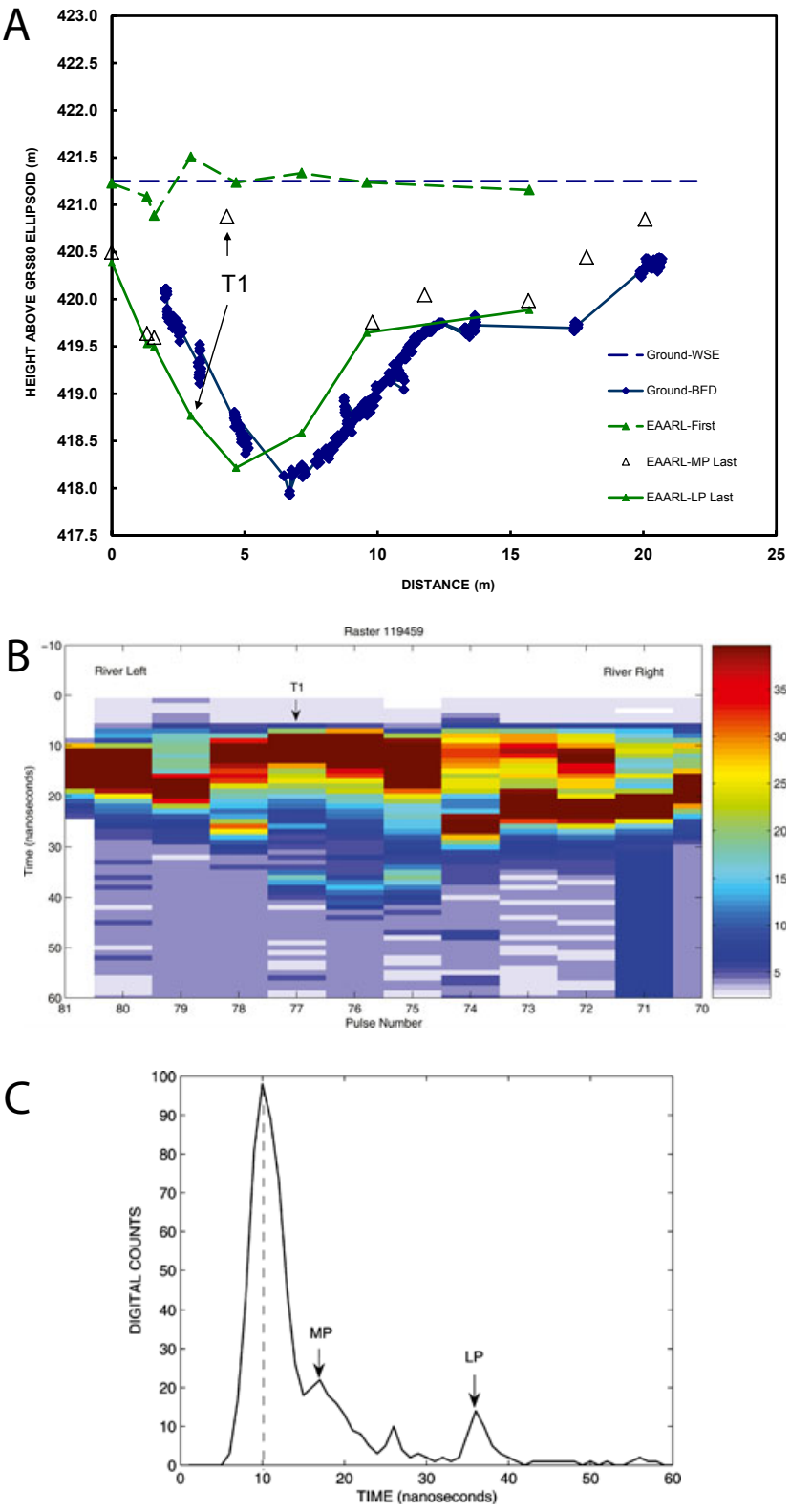

FIGURE 4. Supplementary Information Related to the Trinity River Bathymetric Surveys: (A) Transect T to T′ in the Sheridan Bar Study Site (Figures 3A to 3C) Showing the Ground-Truth Survey and the First and Last Surface Ellipsoid Heights from the EAARL; (B) Plot of Laser Intensity Returned to the Detector Along a Scan Line (raster) Located Near Transect T to T′; (C) Example Waveform from Location T1 Along Transect T to T′. The location of the first return is shown with a dotted line. The locations identified as the last return by the ALPS maximum peak (MP) and last peak (LP) processing algorithms are shown with arrows.

along the channel margins. We believe that the error in these points are due to the algorithm incorrectly identifying inflections of trailing noise and can be reduced by increasing the threshold value for bottom detection. The effect of selection of the threshold value is illustrated and discussed in more detail for the Colorado River survey.

The precision of the first-surface return in detecting the water surface is also shown in Figure 4A. The first-surface elevation was seen to have a large variation, 0.62 m. This difference was observed between adjacent pulses along the same scan line. It could be argued that further processing using automatic filtering or manual editing could be used on a dataset of greater spatial density to identify and eliminate these outliers or the dataset could be reprocessed using alternative bathymetric parameters. To address these potential concerns with the intricacies of processing the returns, we examined a deliverable dataset from the Klamath.

Klamath River – Tree of Heaven Site

As mentioned previously, the Tree of Heaven site EAARL and ground survey were not collected concurrently but we do not believe that gross changes in the river bottom topography, and hence the location and depths of pools, occurred between the surveys. This is based on comparison between surveys collected by the Bureau of Reclamation in this area in October of 2009 (Travis Bauer, USBR, 2009, unpublished data) and the ground-truth survey collected in August of 2010. The discharges were not considerably different between the time of the EAARL survey and the ground survey 45 and 40 m^3/s, respectively. As was done for the Sheridan Bar site, we removed vertical bias from the two surveys by comparing EAARL first-surface elevations collected on a dirt road with adjacent ground survey points. The EAARL survey was processed by the USGS St. Petersburg office with the version of ALPS that included the LP bathymetric algorithm and is shown in Figure 5A. This survey used the same bathymetric parameters as were used in the Trinity survey including a threshold value of 3 for bottom detection and underwent filtering during processing. Our ground-truth sonar survey, Figure 5B, mapped a deep (>3 m) pool in the reach. We compared the surveys along a transect line, K to K′, across a pool by selecting and plotting the EAARL and ground-surveyed sonar points along the transect line. The majority of the EAARL last-return points have a bottom height above the actual ground-truth-surveyed river bottom height (Figure 6A). As with the Trinity River, we selected a laser raster collected across a pool, 120140, to show the relative intensity of laser energy reflected through the water column (Figure 6B). Higher-intensity reflections are observed high in the water column in pulses 63 to 67 but no significant subsequent reflections are observed in the raster. The waveform marked with a "K1" was examined as it was located in one of the deepest portions

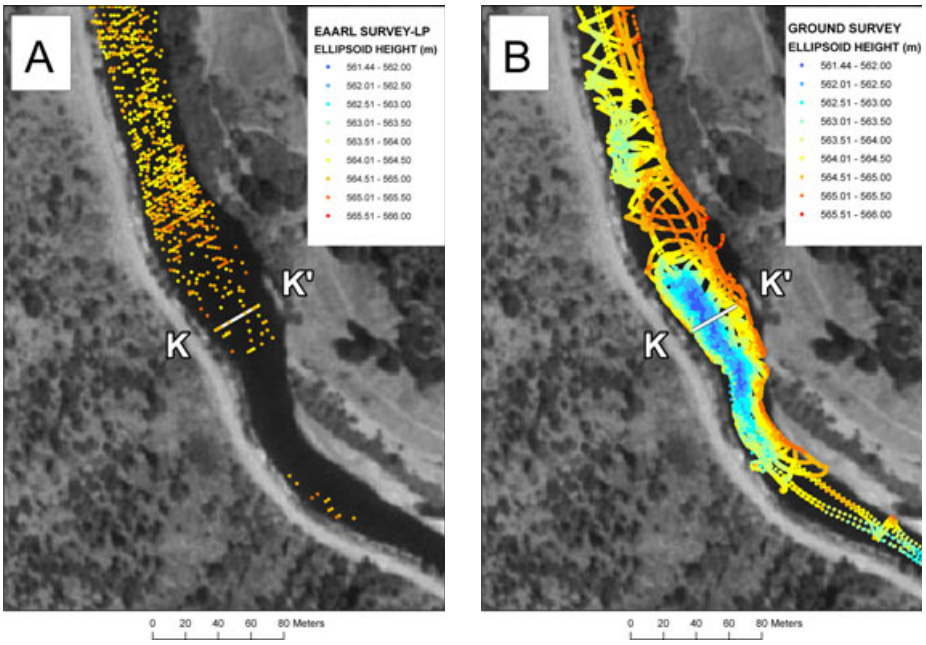

FIGURE 5. Bathymetric Surveys of the Klamath River: (A) Bathymetric Points Collected with the EAARL and Processed Using the Last Peak Bathymetry Algorithm; (B) Bathymetric Points Collected with a Ground Survey. Tree of Heaven study site, Klamath River, California. Flow is from lower right to upper left.

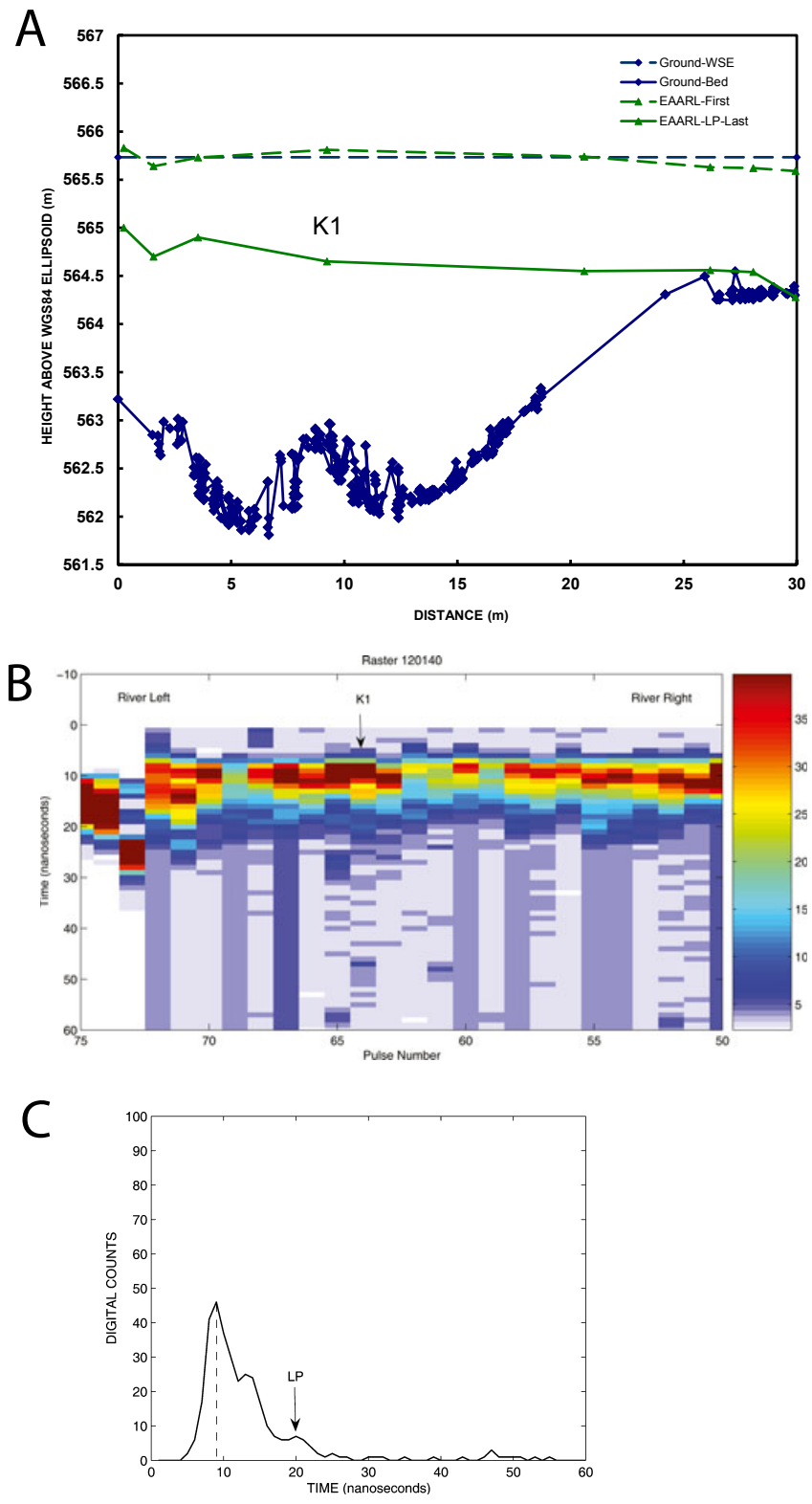

FIGURE 6. Supplementary Information Related to the Klamath River Bathymetric Surveys: (A) Transect K to K′ in the Tree of Heaven Study Site (Figures 5A and 5B) Showing the Ground-Truth Survey and the First and Last Surface Ellipsoid Heights from the EAARL; (B) Plot of Laser Intensity Returned to the Detector Along a Scan Line (raster) Located Near Raster Plot Located Along Transect K to K′; (C) Example Waveform from Location K1 Along Transect K to K′. The location of the first return is shown with a dotted line. The location identified as the last return by the ALPS last peak (LP) processing algorithms is shown with an arrow.

of the transect (Figures 6A and 6C). The last return in this waveform was identified at 20 ns and at a magnitude of 7 digital counts. Given this bottom location, the depth computed by the EAARL is smaller than the ground-truth data would indicate. A very weak reflection of 3 digital counts is observed at 47 ns. However, the threshold value would have needed to be reduced to 2 to select this inflection and if this location was determined to be the bottom, it would be calculated to be almost 1.3 m below the elevation of the ground-truth survey. So it can be only assumed that this inflection represents trailing noise in the waveform. The points provided in the deliverable are relatively sparse in the Klamath dataset (Table 3) and specifically in the region of the transect selected in the pool. However, a shallower pool 80 m downstream of the transect is also not resolved in a location where a somewhat higher density of EAARL points were present.

Turbidity values and suspended sediment concentrations measured at the Tree of Heaven site during the EAARL flight were relatively low (Table 2). An analysis was performed on water samples taken from upstream and downstream of the Indian Creek tributary, approximately 40 km downstream of the Tree of Heaven site. These samples indicated that the dissolved organic matter (DOM) in the Klamath main stem was diluted by tributary water. As compared with the Indian Creek tributary, the absorption at the 532-nm wavelength for the water sample obtained in the Klamath was three times greater. The amount of DOM was not especially high in this location; DOM could be inferred to be a few mg/l based on the absorbance at the 254-nm wavelength, ~0.1 (USGS, 2010, unpublished data). However, field observations made at the time of the EAARL survey lead us to speculate that the reflectivity of the bottom could have been reduced by the presence of algae. Overall, the poor EAARL survey results at the Tree of Heaven site may be a combination of absorption of the laser energy by the water column and the low albedo of the substrate, which dictated that much of the laser energy that did reach the bottom was not reflected to the EAARL detector by the river bed. Not surprisingly, the statistical comparison between the Klamath River surveys indicates, relative to the Trinity River, a high magnitude of ME, RMSE, and SD: 0.32, 0.76, and 0.68 m, respectively (Table 4).

Colorado River – Site Downstream of the Confluence of the Blue and Colorado Rivers

A transect downstream on the Colorado River of the confluence of the Blue and Colorado Rivers was chosen to examine the mapping accuracy of the EAARL. We first processed the EAARL survey with the MP bathymetry algorithm (Figure 7A). Because of the high density of survey data, a random consensus filter was used on the point cloud in ALPS to remove outliers that exceeded a given vertical tolerance, 20 cm in a 5-m cell. The reader is referred to Bonisteel *et al.* (2009) for more details regarding the automatic filters available in ALPS. As with the Trinity and Klamath Rivers, a relatively flat surface, in this case a gravel parking lot located between the rivers, was used to identify and reduce vertical bias between the first-surface elevation of the EAARL and the ground surveys. The sonar ground survey defined a pool along the left bank that was over 1.5 m in depth (Figure 7B). The EAARL survey defined the general location of the pool but the bottom elevations computed from the EAARL were much more variable than those from the ground survey. This survey was then reprocessed with the LP bathymetry algorithm and a threshold of 5 digital counts (Figure 7C). This was 2 digital counts higher than what was used for the Trinity and Klamath surveys. The value was increased because, at a threshold setting of 3, the depth over shallow bars in the channel were overpredicted, due to trailing noise detected as bottom. We compared the surveys along a transect line, C to C′, through the pool by selecting and plotting the EAARL and ground-surveyed sonar points within 0.5 m of the transect line (Figure 8A). Many waveforms returned from the pool and processed with the MP algorithm, like the one identified with a "C1," measured the river bed much higher than the corresponding ground-truth measurements. We also plotted a raster that overlapped the transect (Figure 8B). In this plot, high-intensity reflections are observed in the water column similar to the Trinity and Klamath Rivers (Figures 4B and 6B). The bottom reflection in the waveform was found at 15 ns in what appears to be a component of the water-column turbidity reflection (Figure 8C). Closer examination of this waveform reveals a weaker inflection of 10 digital counts at 24 ns. This inflection was identified as the bottom with the LP algorithm. A similar effect of increased range and deeper depth using the LP algorithm was also observed in waveform T1 in the Trinity River survey (Figure 4C).

Although the average of the EAARL first-return elevations in Figure 8A are identified 0.17 m below the ground-surveyed water surface, subsequent reflections were identified by the processing algorithms as the last-return track with the shoaling of the bottom to the right bank. The first-surface elevation measurements along this transect are from multiple laser scans and flightlines over this reach. When compared with the wading measurements made in the Blue/Colorado confluence, the EAARL data pro-

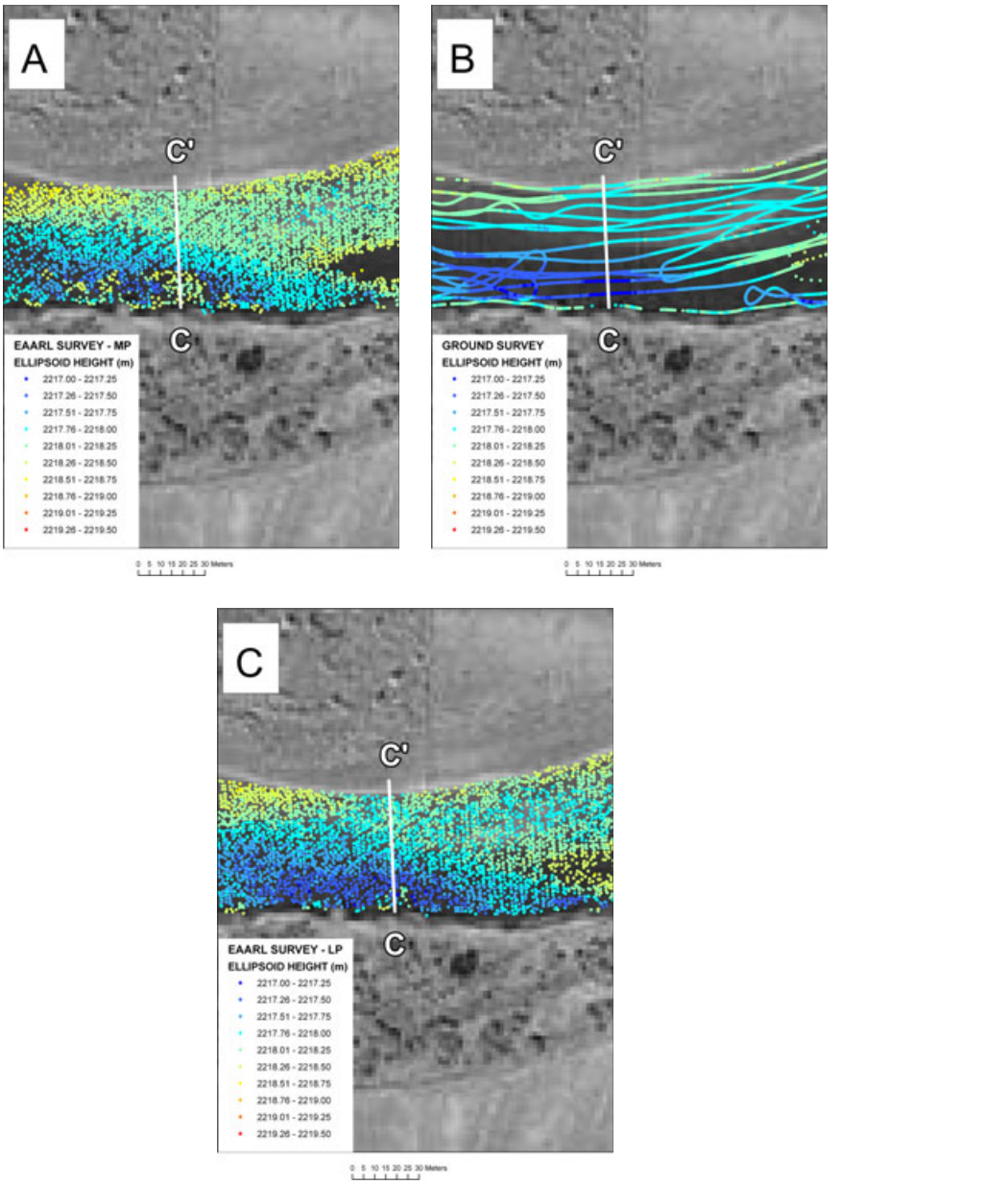

FIGURE 7. Bathymetric Surveys of the Colorado River: (A) Bathymetric Points Collected with the EAARL and Processed with the ALPS Maximum Peak Bathymetry Algorithm; (B) Bathymetric Points Collected with Ground-Truth Surveys; (C) Bathymetric Points Collected with the EAARL and Processed with the ALPS Last Peak Bathymetry Algorithm. Along the Blue/Colorado confluence study site, Colorado River, Colorado. Flow is from right to left.

cessed with the LP algorithm and a threshold of 5 had an ME of 0.07 m and an RMSE of 0.14 m (Table 4). The comparison of sonar measurements to the same EAARL data showed an ME of 0.08 m and an RMSE of 0.15 m.

Since the bathymetric parameters used in ALPS can have a profound effect on the accuracy of the data produced, we examined the effect of varying the threshold parameter used in the LP algorithm. The Blue and Colorado Rivers dataset was first processed with the threshold parameter set at 3. Although this relatively low setting was not found to enhance the recovery of data in pools on the Klamath River, it showed some promise in improving the identification of bottom reflections in the Sheridan Bar pool on the Trinity River. When applied on the Colorado River, we found that when the threshold was set to 3 the bathymetry of the pool was enhanced over the MP approach but that this came with some cost. This threshold setting caused an overprediction of depths

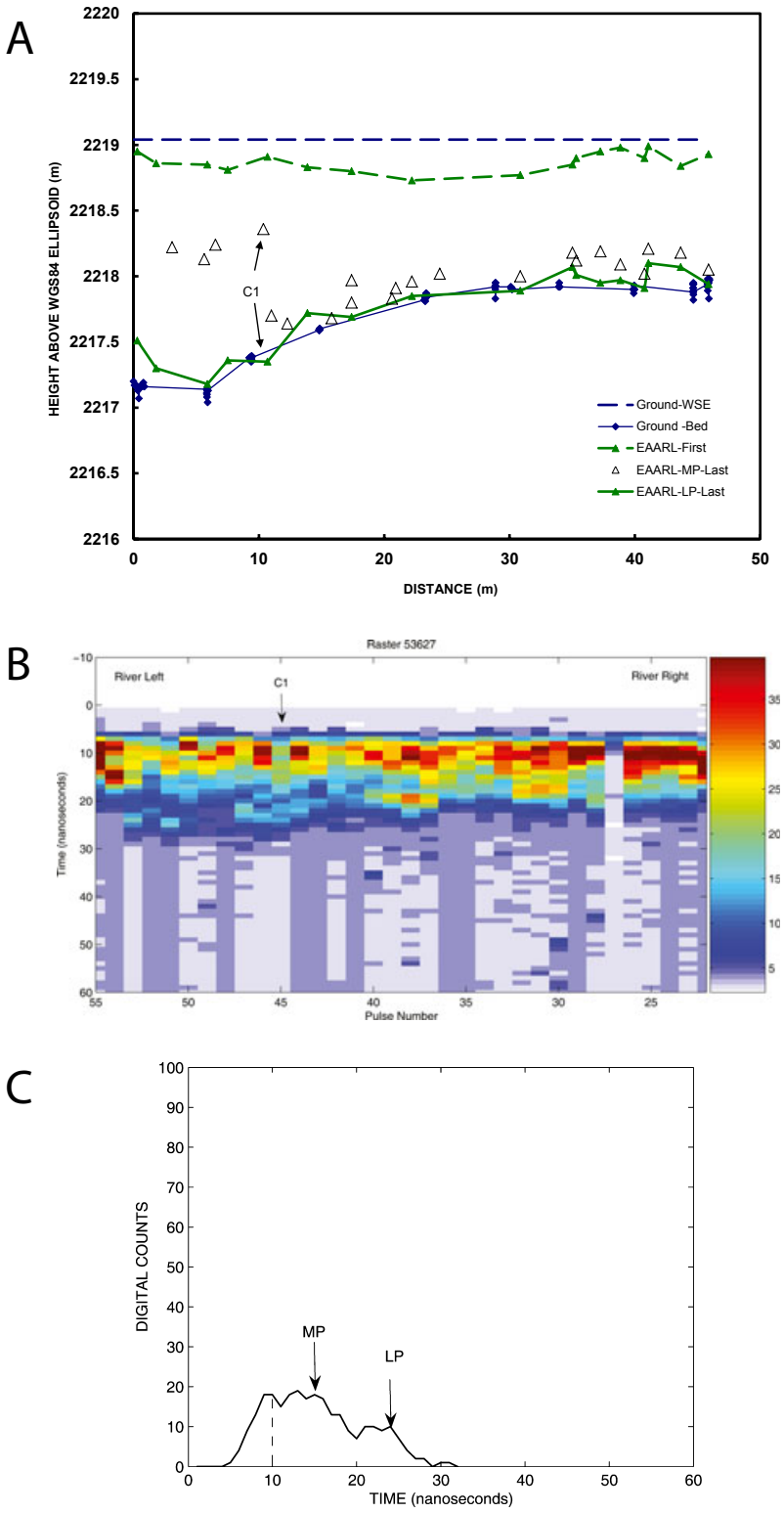

FIGURE 8. Supplementary Information Related to the Colorado River Bathymetric Surveys: (A) Transect C to C′ Through the Blue/Colorado Confluence Study Site (Figures 7A to 7C) Showing the Ground-Truth Survey and the First and Last Surface Ellipsoid Heights from the EAARL; (B) Plot of Laser Intensity Returned to the Detector Along a Scan Line (raster) Located Near Transect C to C′; (C) Example Waveform from Location C1 Along Transect C to C′. The location of the first return is shown with a dotted line. The locations identified as the last return by the ALPS maximum peak (MP) and last peak (LP) processing algorithms are shown with arrows.

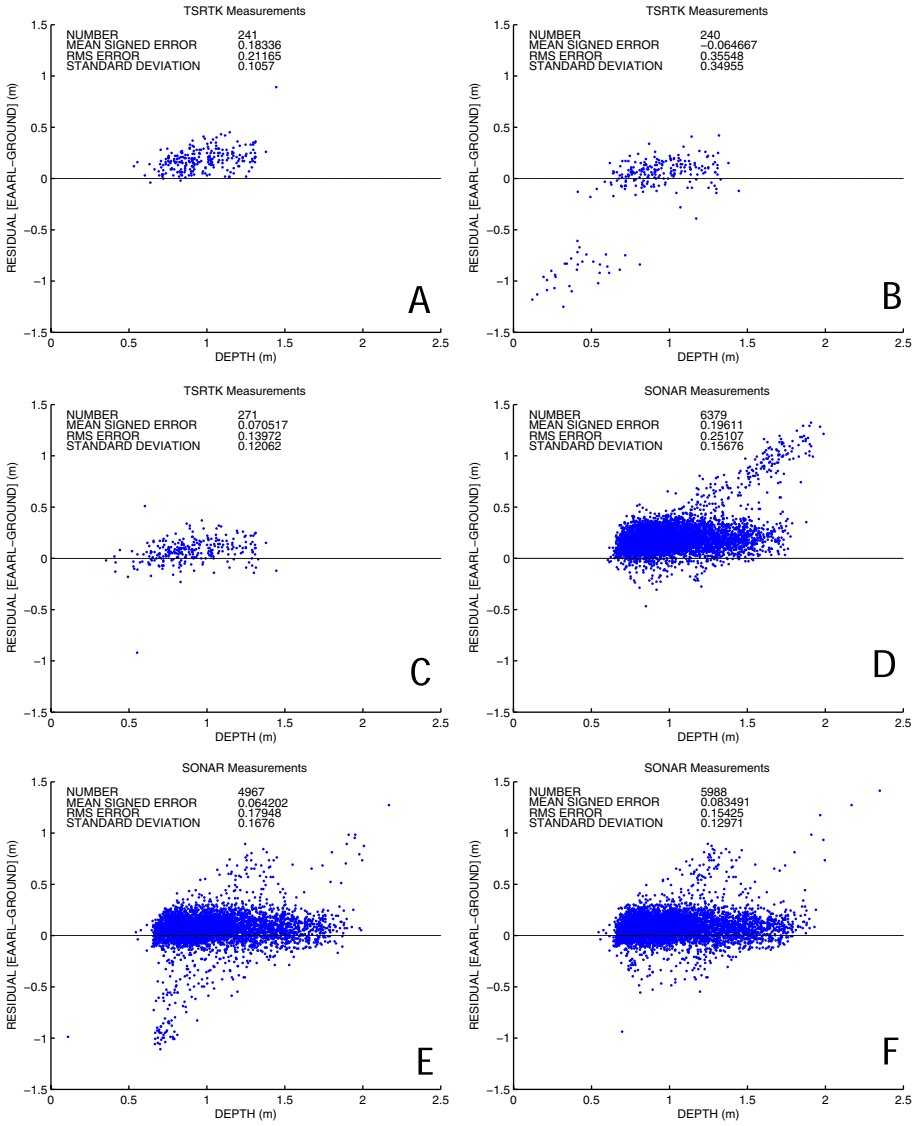

FIGURE 9. Comparisons of Bathymetric Points Collected with Conventional Surveys and Those by the EAARL Using Various Processing Algorithms: (A) Comparison of River Channel Topographic Points Collected with Total Station and RTK GPS (TSRTK) and Adjacent (<0.5 m) EAARL Points Processed with the Maximum Peak Algorithm in ALPS; (B) Comparison of River Channel Topographic Points Collected with Total Station and RTK GPS (TSRTK) and Adjacent (<0.5 m) EAARL Points Processed with the Last Peak Bathymetry Algorithm in ALPS Using a Threshold of 3 Digital Counts; (C) Comparison of River Channel Topographic Points Collected with Total Station and RTK GPS (TSRTK) and Adjacent (<0.5 m) EAARL Points Processed with the Last Peak Bathymetry Algorithm in ALPS Using a Threshold of 5 Digital Counts; (D) Comparison of River Channel Topographic Points Collected with Sonar and Adjacent (<0.5 m) EAARL Points Processed with the Maximum Peak Algorithm in ALPS; (E) Comparison of River Channel Topographic Points Collected with Sonar and Adjacent (<0.5 m) EAARL Points Processed with the Last Peak Bathymetry Algorithm in ALPS Using a Threshold of 3 Digital Counts; (F) Comparison of River Channel Topographic Points Collected with Sonar and Adjacent (<0.5 m) EAARL Points Processed with the Last Peak Bathymetry Algorithm in ALPS Using a Threshold of 5 Digital Counts.

in shallow areas. This is because noise in the trailing edge of the waveform above the threshold of 3 triggered the detection of a false bottom. This effect can best be seen when the EAARL data are compared with adjacent ground-truth wading measurements made with the RTK GPS and TS. Figure 9A shows the errors as a function of depth for EAARL points that were paired wading measurements that were within 0.5 m and processed using the MP algorithm. The ME of the points was 0.18 m and the SD was 0.11 m. When processed with the LP algorithm and a threshold value of 3, the ME decreased to 0.06 m but the SD increased to 0.35 m (Figure 9B). The points lying below the line of perfect agreement indicate comparisons where the EAARL is predicting an elevation below the neighboring ground-truth point.

These outliers were also observed in shallow areas in the Trinity River (Figure 3C). When the threshold value was increased to 5, the number of shallow points misidentified as deep were reduced and the ME increased to 0.07 m and the SD was reduced to 0.12 m (Figure 9C). Increasing the threshold value to 5 did not affect the lower limit of elevations that could be reliably detected. The same relationship between processing algorithms and threshold settings was observed over a wider depth range for the paired sonar points (Figures 9D to 9F).

DISCUSSION AND CONCLUSIONS

Currently, river mapping with bathymetric LiDAR could be described as being in an advancing experimental phase. Although a few specialized hardware and software platforms capable of collecting and processing bathymetric LiDAR are operational and available, the performance and survey accuracy can be influenced by environmental conditions and signal-processing challenges. The field trials of the EAARL system described herein serve to highlight how these factors can influence the accuracy of the surveys and provide an empirical perspective to inform potential users of the technology. These observations are also intended to help advance processing methods for bathymetric waveforms. Each field site posed unique environmental conditions, and the EAARL system and ALPS software (using uniform bathymetric parameters) performed with varying degrees of accuracy under each set of conditions.

In the pool adjacent to Sheridan Bar on the Trinity River, it was apparent that many laser pulses transmitted into the pool were either scattered before reaching the bottom of the pool or returned insufficient energy from the bottom for the processing algorithm to detect that energy as a distinct bottom return. The laser energy that was identified by the processing algorithm as the bottom was more often generated by reflectors higher in the water column. We observed during the sonar surveys that occasionally the sonar would lose the bottom signal in the pool and suspected that turbulence and aeration may be the cause. It is possible that entrained air and turbulence in the pool were responsible for these "false-bottom" reflections. In an evaluation of the EAARL system in the Deadwood and South Fork of the Boise River, Skinner (2011) attributed whitewater or bubbles in the water column as a possible cause for the reduction in water depths measured by the EAARL.

The Klamath River EAARL survey was unable to define the pool at the Tree of Heaven study site. Water clarity would seem at first blush to be a likely cause. Turbidities between 4.2 and 19.3 NTU were identified by Skinner (2009) as a range over which EAARL system performance became affected along the lower Boise River. However, our data indicated an apparent absence of scattering material in the water column, low turbidity (3 NTU) and suspended sediment concentration at the field site, and low DOM at a downstream site. This has led us to speculate that low-bottom albedo may also be a contributing factor to the system's inability to resolve deeper pools. The dark basaltic substrate and algae on these submerged surfaces would be more absorptive of the EAARL laser energy than brighter and cleaner substrates with higher reflectance.

The comparison of the wading and sonar measurements with the EAARL survey collected at the Blue/Colorado confluence site collectively show the lowest ME, a measure of bias, and also relatively low values of statistical dispersion (RMSE) for the sonar measurements. Although the location of pools was apparent in the EAARL-derived bathymetric maps of this reach, when processed with the MP algorithm the soundings in the pools were also seen to be interspersed with false-bottom reflections higher in the water column. The weak-bottom inflections in these waveforms indicated that the laser pulse was penetrating close to the bottom and the bottom detection in these waveforms could be extended by using the LP algorithm. However, the challenge in using this algorithm lies in the selection of a threshold low enough to detect a muted bottom signal but high enough to avoid identify trailing noise in shallow areas as bottom. Although turbidity values were unfortunately not collected concurrently with the EAARL measurements, subsequent measurements made at similar suspended sediment concentrations indicated that values approaching as high as 6 NTU may be sufficient for the system to operate effectively.

As a research instrument, the EAARL has shown potential for mapping in-channel topographies, with the important proviso that the optical properties of the water column and the albedo of the bottom permit bed reflections of significant strength to be detected by the sensor and identified by the processing algorithms. Bonisteel *et al.* (2009) identified that the maximum depth the EAARL could penetrate as 1.5 times the Secchi disk depth or approximately 20 m in clear water. However, the EAARL was designed to primarily survey coral reefs and marine environments. To assist in quantifying limitations in riverine environments, future work and field evaluations would benefit from the use of field spectroscopy at the time of an EAARL survey (Legleiter *et al.*,

2011) to quantify both attenuation by the water column at the 532-nm EAARL laser wavelength and the reflectance of various substrate types. Another useful field experiment would involve flying or positioning the system on the ground over pools of water of varying depths, turbidities, and bottom reflectivities. These comparisons could take a more piecemeal approach to first isolate and then examine the interplay of the multiple factors influencing laser backscatter in shallow riverine environments. These evaluations would also provide ground truth for further testing and development of ALPS waveform-processing algorithms.

At the time of this writing, hardware modifications planned for the next-generation EAARL sensor, EAARL-B, include an order of magnitude increase in laser power from 70 to 700 mJ. To remain eye safe, the laser energy will be divided over three laser spots, with each of the spots retaining the current (~20 cm) size. The net effect will thus be to triple the number of laser samples in each raster or swath. This and other modifications will increase the pulse repetition frequency from 5,000 to 30,000 Hz. This greater rate of sampling will be advantageous in fluvial settings where multiple passes have been used to build up point density. However, an increase in laser power may not necessarily translate into enhanced bottom detection if the river is dominated by scattering and absorption. ALPS and waveform-processing algorithms that can improve the ranging accuracy to shallow-water targets are also continually under development and as shown in this article can have a marked effect on accuracy. Also illustrated in this article is the continued importance of field trials of the EAARL in diverse settings (differing channel morphologies, substrates, and water clarities) to quantify the effect of these hardware and software improvements for mapping fluvial environments.

ACKNOWLEDGMENTS AND DISCLAIMER

The authors would like to thank the following individuals with assistance collecting field data: Brandy Logan, Mary Ann Madej, John Pitlick, Julia Uhlendorf, and Scott Wright. This work was funded by the Office of Naval Research Grant N0001409IP20057, "Computational Modeling of River Flow, Sediment Transport, and Bed Evolution Using Remotely Sensed Bathymetry." Any use of trade, firm, or product names is for descriptive purposes only and does not imply endorsement by the U.S. Government.

LITERATURE CITED

Allouis, T., J.S. Bailly, Y. Pastol, and C. LeRoux, 2010. Comparison of LiDAR Waveform Processing Methods for Very Shallow Water Bathymetry Using Raman, Near-Infrared and Green Signals. Earth Surface Processes and Landforms 35:640-650.

Bailly, J.S., Y. LeCoarer, P. Languille, C. Stigermark, and T. Allouis, 2010. Geostatistical Estimation of Bathymetric LiDAR Errors on Rivers. Earth Surface Processes and Landforms 35:1199-1210.

Bonisteel, J.M., A. Nayegandhi, C.W. Wright, J.C. Brock, and D.B. Nagle, 2009. Experimental Advanced Airborne Research Lidar (EAARL) Data Processing Manual. U.S. Geological Survey Open-File Report, 2009-1078, 38 pp.

Bowen, Z.H., K.D. Bovee, and T.J. Waddle, 2003. Effects of Flow Regulation on Shallow-Water Habitat Dynamics and Floodplain Connectivity. Transactions of the North American Fisheries Society 132(4):809-823.

Bowen, Z.H. and R.G. Waltermire, 2002. Evaluation of Light Distancing and Ranging (LiDAR) for Measuring River Corridor Topography. Journal of the American Water Resources Association 38(1):33-41.

Brasington, J., B.T. Rumsby, and R.A. McVey, 2000. Monitoring and Modelling Morphological Change in a Braided Gravel-Bed River Using High Resolution GPS-Based Survey. Earth Surface Processes and Landforms 25:973-990.

Carbonneau, P.E., S.N. Lane, and N. Begeron, 2006. Feature Based Image Processing Methods Applied to Bathymetric Measurements From Airborne Remote Sensing in Fluvial Environments. Earth Surface Processes and Landforms 31:1413-1423.

Collier, M., R.H. Webb, and J.C. Schmitt, 1996. Dams and Rivers: A Primer on the Downstream Effects of Dams. U.S. Geological Survey Circular 1126.

Feygels, V.I., C.W. Wright, Y.I. Kopilevich, and A.I. Surkov, 2003. Narrow-Field-of-View Bathymetrical Lidar: Theory and Field Test. Proceedings of the Ocean Remote Sensing and Imaging II; SPIE 5155:1-11.

Goodwin, R.A., J.M. Nestler, J.J. Anderson, L.J. Weber, and D.P. Loucks, 2006. Forecasting 3-D Fish Movement Behavior Using a Eulerian-Lagrangian-Agent Method (ELAM). Ecological Modelling 192:197-223.

Guenther, G.C., 2007. Airborne Lidar Bathymetry. *In*: Digital Elevation Model Technologies and Applications: The DEM Users Manual (Second Edition), D. Maune (Editor). American Society for Photogrammetry and Remote Sensing, Bethesda, Maryland, pp. 253-320.

Hicks, D.M., M.J. Duncan, J.M. Walsh, R.M. Westaway, and S.N. Lane, 2002. New Views of the Morphodynamics of Large Braided Rivers From High-Resolution Topographic Surveys and Time-Lapse Video. *In*: The Structure, Function and Management Implications of Fluvial Sedimentary Systems, F.J. Dyer, M.C. Thoms, and J.M. Olley (Editors). IAHS Publication No. 276, Wallingford, pp. 373-380.

Hicks, D.M., U. Shankar, M.J. Duncan, M. Rebuffé, and J. Aberle, 2006. Use of Remote-Sensing With Two-Dimensional Hydraulic Models to Assess Impacts of Hydro-operations on a Large, Braided, Gravel-Bed River: Waitaki River, New Zealand. *In*: Braided Rivers: Process, Deposits, Ecology and Management, G.H. Sambrook Smith, J.L. Best, C.S. Bristow, and G.E. Petts (Editors). Special Publication Number 36 of the International Association of Sedimentologists. Blackwell Publishing, Malden, Massachusetts, pp. 311-326.

Hilldale, R.C. and D. Raff, 2008. Assessing the Ability of Airborne LiDAR to Map River Bathymetry. Earth Surface Processes and Landforms 33:773-783.

Höfle, B., M. Vetter, N. Pfeifer, G. Mandlburger, and J. Stötter, 2009. Water Surface Mapping From Airborne Laser Scanning Using Signal Intensity and Elevation Data. Earth Surface Processes and Landforms 34:1635-1649.

Holling, C.S., 1978. Adaptive Environmental Assessment and Management. John Wiley, New York, New York.

Huising, E.J. and L.M. Gomes Pereira, 1998. Errors and Accuracy Estimates of Laser Data Acquired by Various Laser Scanning Systems for Topographic Applications. ISPRS Journal of Photogrammetry and Remote Sensing 53:245-261.

Kinzel, P.J., C.W. Wright, J.M. Nelson, and A.R. Burman, 2007. Evaluation of an Experimental LiDAR for Surveying a Shallow, Braided, Sand-Bedded River. Journal of Hydraulic Engineering 133(7):838-842.

Krause, A., P. Wilcock, and D. Gaeuman, 2010. One Hundred and Fifty Years of Sediment Manipulation on the Trinity River, CA. Proceedings of the Joint Federal Interagency Conference 2010, Las Vegas, Nevada.

Lane, S.N., 2006. Approaching a System-Scale Understanding of Braided River Behavior. *In*: Braided Rivers: Process, Deposits, Ecology and Management, G.H. Sambrook Smith, J.L. Best, C.S. Bristow, and G.E. Petts (Editors). Special Publication Number 36 of the International Association of Sedimentologists. Blackwell Publishing, Malden, Massachusetts, pp. 107-135.

Lane, S.N., K.S. Richards, and J.H. Chandler, 1994. Developments in Monitoring and Modelling Small-Scale River Bed Topography. Earth Surface Processes and Landforms 19(4):349-368.

Legleiter, C.J., P.J. Kinzel, and B.T. Overstreet, 2011. Evaluating the Potential for Remote Bathymetric Mapping of a Turbid, Sand-Bedded River 1. Field Spectroscopy and Radiative Transfer Modeling. Water Resources Research 47:W09531, doi: 10.1029/2011WR010591.cd.

Legleiter, C.J. and P.C. Kyriakidis, 2008. Spatial Prediction of River Channel Topography by Kriging. Earth Surface Processes and Landforms 33(6):841-867.

Legleiter, C.J., D.A. Roberts, and R.L. Lawrence, 2009. Spectrally Based Remote Sensing of River Bathymetry. Earth Surface Processes and Landforms 34(8):1039-1059.

Legleiter, C.J., D.A. Roberts, W.A. Marcus, and M.A. Fonstad, 2004. Passive Remote Sensing of River Channel Morphology and In-Stream Habitat: Physical Basis and Feasibility. Remote Sensing of Environment 93:493-510.

Lejot, J., C. Delacourt, H. Piégay, T. Fournier, M.L. Trémélo, and P. Allemand, 2007. Very High Spatial Resolution Imagery for Channel Bathymetry and Topography From an Unmanned Aerial Platform. Earth Surface Processes and Landforms 32:1705-1725.

Li, S.S., R.G. Millar, and S. Islam, 2008. Modeling Gravel Transport and Morphology for the Lower Fraser River, British Columbia. Geomorphology 95(3-4):206-222.

Marcus, W.A. and M.A. Fonstad, 2010. Remote Sensing of Rivers: The Emergence of a Subdiscipline in the River Sciences. Earth Surface Processes and Landforms 35:1867-1872.

Marks, K. and P. Bates, 2000. Integration of High-Resolution Topographic Data With Floodplain Flow Models. Hydrologic Processes 14:2109-2122.

May, C.L., B.S. Pryor, T. Lisle, and M. Lang, 2009. Coupling Hydrodynamic Modeling and Empirical Measures of Bed Mobility to Predict the Risk of Scour and Fill of Salmon Redds in a Large Regulated River. Water Resources Research 45:W05402, doi: 10.1029/2007WR006498.

McKean, J.A., D.J. Isaak, and C.W. Wright, 2008. Geomorphic Controls on Salmon Nesting Patterns Described by a New, Narrow-Beam Terrestrial-Aquatic Lidar. Frontiers in Ecology and the Environment 6(3):125-130.

McKean, J.A., D. Nagel, D. Tonina, P. Bailey, C.W. Wright, C. Bohn, and A. Nayegandhi, 2009. Remote Sensing of Channels and Riparian Zones With a Narrow-Beam Aquatic-Terrestrial LIDAR. Remote Sensing 1(4):1065-1096.

Millar, D., 2008. Using Airborne LIDAR Bathymetry to Map Shallow River Environments: A Successful Pilot on the Colorado River, European Geosciences Union Annual Meeting, April 13-18, 2008, Vienna, Austria.

Mueller, D.S. and C.R. Wagner, 2008. Measuring Discharge With Acoustic Doppler Current Profilers From a Moving Boat: U.S. Geological Survey Techniques and Methods 3A-22, 72 pp. http://pubs.water.usgs.gov/tm/3a22, *accessed* October 16, 2012.

Nayegandhi, A., J.C. Brock, and C.W. Wright, 2008. Small-Footprint, Waveform Resolving Lidar Estimation of Submerged and Sub-Canopy Topography in Coastal Environments. International Journal of Remote Sensing 30(4):861-878.

Nayegandhi, A., J.C. Brock, C.W. Wright, and M.J. O'Connell, 2006. Evaluating a Small-Footprint Waveform Resolving Lidar Over Coastal Vegetation Communities. Photogrammetric Engineering and Remote Sensing 72(12):1407-1417.

Poff, N.L., J.D. Allen, M.B. Bain, J.R. Karr, K.L. Prestegaard, B.D. Richter, R.E. Sparks, and J.C. Stromberg, 1997. The Natural Flow Regime: A New Paradigm for Riverine Conservation and Restoration. Bioscience 47:769-784.

Railsback, S.F., H.B. Stauffer, and B.C. Harvey, 2003. What Can Habitat Preference Models Tell Us? Tests Using a Virtual Trout Population. Ecological Applications 13(6):1580-1594.

Richter, B.D., A.T. Warner, J.L. Meyer, and K. Lutz, 2006. A Collaborative and Adaptive Process for Developing Environmental Flow Recommendations. River Research and Applications 22:297-318.

Skinner, K.D., 2009. Evaluation of LiDAR-Acquired Bathymetric and Topographic Data Accuracy in Various Hydrogeomorphic Settings in the Lower Boise River, Southwestern Idaho, 2007. U.S. Geological Survey Scientific Investigations Report 2009-5260, 12 pp.

Skinner, K.D., 2011. Evaluation of LiDAR-Acquired Bathymetric and Topographic Data Accuracy in Various Hydrogeomorphic Settings in the Deadwood and South Fork Boise Rivers, West-Central Idaho, 2007. U.S. Geological Survey Scientific Investigations Report 2011-5051, 30 pp.

Tayefi, V., S.N. Lane, R.J. Hardy, and D. Yu, 2007. A Comparison of One- and Two-Dimensional Approaches to Modeling Flood Inundation Over Complex Upland Floodplains. Hydrological Processes 21:3190-3202.

Tiffan, K.F., R.D. Garland, and D.W. Rondorf, 2002. Quantifying Flow-Dependent Changes in Subyearling Fall Chinook Rearing Habitat and Stranding Area Using Two-Dimensional Spatially-Explicit Modeling. North American Journal of Fisheries Management 22:713-726.

Trimble Navigation Limited, 1998. Survey Controller Field Guide, Version 7.0. Trimble Navigation Limited, Sunnyvale, California, 94 pp.

U.S. Department of the Interior Bureau of Land Management, 2007. Final Wild and Scenic Eligibility Report, Kremmling and Glenwood Springs Field Offices, 151 pp.

U.S. Fish and Wildlife Service and Hoopa Valley Tribe, 1999. Trinity River Flow Evaluation Final Report. Arcada and Hoopa Valley, California, 309 pp. and appendices.

Waddle, T.J., P. Steffler, A. Ghanem, C. Katopodis, and A. Locke, 2000. Comparison of One and Two-Dimensional Open Channel Flow Models for a Small Habitat Stream. Rivers 7(3):205-220.

Walters, C., 1997. Challenges in Adaptive Management of Riparian and Coastal Ecosystems. Conservation Ecology 1(2). http://www.consecol.org/vol1/iss2/art1, *accessed* October 16, 2012.

Westaway, R.M., S.N. Lane, and D.M. Hicks, 2003. Remote Survey of Large-Scale Braided, Gravel Bed Rivers Using Digital Photogrammetry and Image Analysis. International Journal of Remote Sensing 24:795-816.

Williams, G.P. and M.G. Wolman, 1984. Downstream Effects of Dams on Alluvial Rivers. U.S. Geological Survey Professional Paper 1286.

Winterbottom, S.J. and D.J. Gilvear, 1997. Quantification of Channel Bed Morphology in Gravelbed Rivers Using Airborne Multispectral Imagery and Aerial Photography. Regulated Rivers: Research and Management 13(6):489-499.

Wright, C.W. and J.C. Brock, 2002. EAARL: A LIDAR for Mapping Coral Reefs and Other Coastal Environments. Seventh International Conference on Remote Sensing for Marine and Coastal Environments, National Oceanic and Atmospheric Administration, Miami, Florida, 8 pp.